THE PUBLISHING HOUSE
OF THE ROMANIAN ACADEMY

PROCEEDINGS OF THE ROMANIAN ACADEMY, Series A,
Volume 17, Number 3/2016, pp. 259–266

ELECTRICAL CARDIOMETRY SIMULATION FOR THE ASSESSMENT OF CIRCULATORY PARAMETERS

Alexandru Mihail MOREGA[1], Alin Alexandru DOBRE [2], Mihaela MOREGA [3]

[1] "Politehnica" University of Bucharest and the Institute of Statistical Mathematics and Applied Mathematics "Gheorghe Mihoc – Caius Iacob" of the Romanian Academy of Science, Bucharest, Romania
[2] National Institute for Biodynamics, Bucharest, Romania
[3] University "Politehnica" of Bucharest, Romania
Corresponding author: Alexandru Mihail MOREGA, E-mail: amm@iem.pub.ro

Abstract. Non-invasive monitoring techniques for the assessment of various cardiovascular parameters are increasingly accepted as current medical practice. Perceived as harmless and safe tests, offering reliable medical data regarding circulatory and cardiac conditions on relative low costs, they are also easily accepted by the patients. Solving the direct problem in electrical cardiometry by numerical simulation and analysis of the solution represent the main objectives of the study developed here. A mathematical model of the aortic blood flow is coupled with the electrical impedancemetry problem. The dynamics of the aortic blood electrical conductivity is considered and the computational model is derived from a realistic anatomical structure representing the human thorax, which is produced by reconstruction techniques from medical images. It is further solved by the finite element technique. The direct problem of electrical cardiometry applied in the study aims at assessing the sensitivity of hemodynamic parameters to flow characteristics and dynamic electrical properties of the blood through the aortic path; the flow and conductivity change are synchronized with the cardiac cycle.

***Key words**:* bioimpedance, computer assisted cardiology, dynamic conductivity of blood, electrical cardiometry, finite element analysis.

1. INTRODUCTION

Measurements of the electrical impedance commonly give information on the composition of the analyzed volume, based on the variability of dielectric properties; frequency dependence of these properties is used to increase the accuracy of the method. When exposed to low frequency electric field, human tissues behave similar to conductive materials. Dispersion of global impedance measured on a certain body volume occurs due to variability in electrical conductivity of subdomaines (tissues). Biophysical characteristics of blood (pulsatile variations of fluid volume through the arterial tree and dynamics of electrical conductivity of blood) are commonly considered the most sensitive quantities in the variation of the *Thoracic Electrical Bioimpedance* (TEB) [1], measurable by unobtrusive, non-invasively techniques: *Impedance CardioGraphy* (ICG), and *Electrical CardioMetry* (ECM).

Non-invasive impedance measurement in TEB techniques is an inexpensive, feasible method for cardiac investigation and diagnosys [1, 2], and for continuous monitoring the aortic blood flow in a clinical environment [3, 4]. TEB dynamics could be synchronized and correlated with the *Electrocardiographic* (ECG) and *Respiratory* signals, aiming to offer sufficient while consistent data for the assessment of several cardio-respiratory indices: *Stroke Volume* (SV), *Cardiac Output* (CO), *Systemic Vascular Resistance* (SVR), *Peak Aortic Acceleration of blood* (PAA), *Flow Time* (FT), *Velocity of the Blood Flow* (VBF) [5, 6].

Electrical CardioMetry (ECM) emerged approx. ten years ago, associated to a patented device [7], trademarked by Cardiotronic, Inc. (www.cardiotronic.net), and its medical application evolved from general cardiac output assessment [6] to myocardial ischemic injury detection [8]. TEB uses two dual electrodes – a pair attached to the left side of the neck and the other placed on the lower thorax. An electric current $i(t)$ of relatively low frequency (< 1 MHz) and low amplitude (< 0.5 mA) is injected via the outer electrodes and a voltage $u(t)$ is measured at the inner electrodes; the ratio of the two signals and its derivative are computed on-

line. It has become common practice to associate TEB with the so-called *derived bioimpedance,* i.e. the inverse of the bioimpedance waveform (an admittance), perceived as a *measure-of-conductivity* waveform $dZ(t) = 1/Z(t) = i(t)/u(t)$, and to its time derivative, $dZ(t)/dt$, understood as a *change-of-conductivity* waveform.

The measurement senses changes in the aortic blood electrical conductivity during a cardiac cycle, when successive blood flow stages occur, each marked by a switch in orientation of *red blood cells* (RBC). Figure 1 (after [6]) shows the correlation between cardiovascular indices, revealed by *the electrocardiogram* (ECG) synchronized with *the derived bioimpedance,* its time-derivative $dZ(t)/dt$ and *the pulse plethysmograph* waveforms. Two drawings attached to the waveforms suggest switching in RBCs orientation with the aortic blood flow, as reason for the change in electrical conductivity. *Diastolic period* corresponds to low electrical conductivity (left drawing, just before aortic valve opening, when RBCs are randomly distributed and the electrical resistance is high), while *systolic period* favors the rise of electrical conductivity (right drawing, where RBCs are aligned streamwise, shortly after aortic valve opening, and change their shape to favor flow and electric conduction).

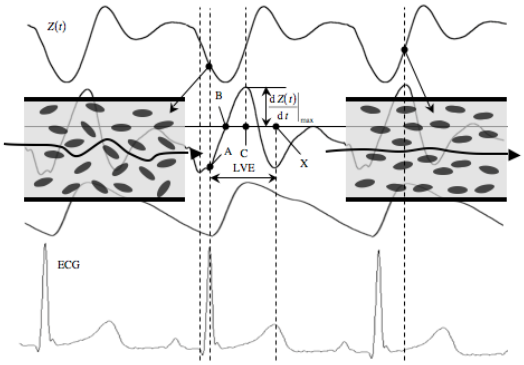

Fig. 1 – Syncronized recordings of ECG, pulse plethysmogram and impedance waveforms with the computed derived bioimpedance; the two drawings show the red blood cells orientation in the aorta prior to and shortly after aortic valve opening (images compiled after [6]).

The same principle is applied for cardiac output assessment from brachial artery cardiometry measurements [9]. Specialized literature offers elaborated theories based on experiments treating interactions between Poiseuille type blood flow and conductivity, e.g. [10]. This study introduces a mathematical model for the ECM medical procedure, and the electric field associated to the bioimpedance measurement, where the unsteady pulsating aorta flow is considered in connection with a proposed model for the change in the electrical conductivity of the blood. The model is analyzed by the finite element method (FEM) in Comsol Multiphysics implementation [11].

2. PARTICULAR FEATURES OF THE NUMERICAL SIMULATION

The numerical simulation considers a more realistic human anatomical model (upper half of the body) with non-homogeneous structure, subjected to the ECM procedure. TEB signal is generated taking into account the dynamics of the electrical conductivity of blood, correlated with the flow. These two particular characteristics of the numerical model are detailed below.

a) translucent upper body with internal organs of the thorax; the electrodes are visible on the left side.

b) FEM mesh, made of approximately 565,000 tetrahedral elements.

Fig. 2 – The computational domain reconstructed from MRI images.

Realistic computational models are presently the standard for meaningful results to medical problems, from the numerical simulation perspective. Image acquiring equipments (CT and MRI scanners) provide personalized sets of 2D slices. Specialized software morphs them afterwards and complements the internal anatomy connections, to reconstruct 3D anatomical volumes and to segment out anatomic regions of interest. For this study, a cut-out-of-the-body 3D geometry is generated using approximately 500 accurate, high resolution MRI images of the whole body in the DICOM (*Digital Imaging and Communications in Medicine*) specific medical format; the source of the image dataset is [12] and the reconstructed anatomy is drawn in Fig. 2a, after using specialized software [13, 14]. The following stage was the generation of a suitable FEM mesh (Fig. 2b). Details on the numerical processing of the images are given in previously reported work [15]. The final geometry of the upper human body presented in Fig. 2, is used in the simulation of ECM. An equivalent conductivity for the blood is adopted in this study, according to Visser [16], Gaw *et al*. [17] and Hoetinc *et al.* [10]. RBCs floating in plasma are assimilated with a dilute suspension of ellipsoidal particles. The electrical conductivity of such a structure exposed to time-harmonic electric field (of relatively low frequency) is provided by Visser [16], which uses the classical Maxwell-Fricke model.

Blood flowing through the aorta is treated similarly as the suspension described above, flowing through a cylindrical tube. The pulsatile flow is characterized by the synchronism of the bioimpedance and flow dynamic changes during flow acceleration versus an exponential decay in orientation of ellipsoids during flow deceleration; the time constant of the decelerating process is in the order of 10^0–10^2 s. These hypotheses were already introduced and tested in earlier demonstrations of TMB numerical simulation [5, 18], while [10] clearly indicates the significance of blood resistivity changes for signals acquired in transbrachial electrical bioimpedance velocimetry. Based on previous considerations, the dynamics of the electrical conductivity synchronized with the flow could be simulated by a mathematical model, already applied in [5] and [18], based on elements introduced by Hoetinc *et al*. [10] and by Gaw *et al*. [17]. Local blood electrical conductivity is expressed in [10] thorough

$$\sigma_b = \sigma_{pl} \frac{1-H}{1+(C-1)H}, \tag{1}$$

where σ_b and σ_{pl} [S·m^{-1}] are the electric conductivities of blood and plasma, H is the hematocrit, C a geometry factor for the RBC; in the round tube theory [17] it is a function of the tube radius and when evaluated for a cylinder of radius $r = r_0$ its expression is

$$C(r_0) = f(r_0)\cdot C_b + \left[1 - f(r_0)\right]\cdot C_r, \qquad C_r = (C_a + 2C_b)/3,\ C_a = 1/M,\ C_b = C(r_0) = 2/(2-M), \tag{2}$$

where M depends on the geometry of RBCs, assimilated with ellipsoids of axes $a < b$; if $\cos\varphi = a/b$,

$$M = \cos\varphi\cdot(\varphi - \sin 2\varphi)/\sin^3\varphi. \tag{3}$$

In our study, calculations where performed for a/b = 0.38 (an average value proposed for RBCs by Gaw *et al.* [17]), which leads to the simplified expression $M \cong a/b$. The approximate expression proposed by Gaw *et al*. [17] for the *orientation rate* in eq. (2) is

$$f(r) = \frac{n}{n_0}\frac{\theta_0^{-1}(r)}{\theta_d^{-1}(r) + \theta_0^{-1}(r)}, \tag{4}$$

where r is the radius of the cylindrical duct (in our model $r = r_0$), n is the number per unit volume of RBCs with stable orientation (parallel to the flow), n_0 is the total number per unit volume of RBCs, θ_0 [s] is the time constant for cell orientation (cells changing from random to aligned orientation) and θ_d is the time constant for cells randomization (or cell disorientation). θ_0 is proportional to the inverse of the shear rate and θ_d is proportional to the inverse of the square root of the shear rate.

The deformation of RBCs in shear flow is related to the resulting shear stress in the fluid. The shear rate, τ_w [N/m^2] – a local quantity – is approximated here, in the order of magnitude sense, by the average friction factor [19]. In fully developed Hagen-Poiseuille flow through a round tube

$$\tau_w = \mu\left(-\frac{\mathrm{d}u}{\mathrm{d}r}\right)\Bigg|_{r=r_0} = 4\eta\frac{U}{r_0}, \tag{5}$$

where u [m/s] is the local, streamwise velocity, U [m/s] is the average velocity of the stream, η [Pa·s] is the dynamic viscosity of blood. The blood vessel simulated in our study is not a cylinder, but the aorta is realistically represented by reconstruction from MRI slices. To overcome this difficulty, the mathematical model described above is further applied to a so called *equivalent round tube* simulating the aorta as follows:

– the radius r_0 results by assimilating the average cross-section area of the aorta, to a circular shape;
– the tube length results as the ratio between the aorta volume and its average cross-section area;
– the average velocity of the stream U is computed out of the mass flow rate.

Figure 3 shows the equivalent shear rate τ_w that resulted from our numerical simulation. The resulted range of the shear rate, $\tau_w > 0.1$ N/m^2 confirms the option for the mathematical model of the electrical conductivity of blood (1) predicted by Hoetink *et al*. [10].

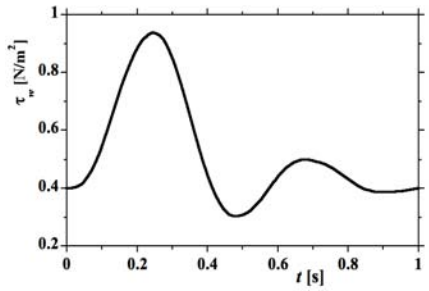

Fig. 3 – The equivalent shear rate for blood flow through aorta, τ_w.

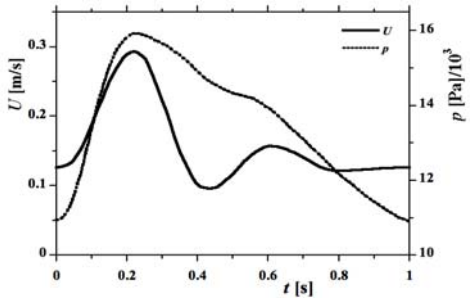

Fig. 4 – Velocity and pressure set as boundary conditions.

3. NUMERICAL MODEL OF ECM

Two physical phenomena are coupled for the simulation of ECM – the pulsatile blood flow in the aorta (thoracic segment significant for ECM) and the electric field distribution in the whole computational domain, due to the electric current, crossing the body between the outer electrodes (Fig. 2a).

The blood flow problem is built on the following assumptions:

– the blood is treated as a Newtonian fluid; a satisfactory hypothesis for large arteries considers that it has constant properties;
– the blood flow is pulsatile, laminar and incompressible.

Two equations make the mathematical model, as already stated in [20, 21, 22] for blood flow through large ("resistive" type) vessels: *momentum balance* (Navier-Stokes) and *mass conservation law*

$$\rho\left[\frac{\partial \mathbf{u}}{\partial t}+(\mathbf{u}\cdot\nabla)\mathbf{u}\right]=\nabla\left[-p\mathbf{I}+\eta\left(\nabla\mathbf{u}+(\nabla\mathbf{u})^{T}\right)\right],\quad \nabla\cdot\mathbf{u}=0, \tag{6}$$

where the mass density of blood is $\rho = 1050$ kg/m^3, $\mathbf{u}$ [m/s] represents the velocity field, p [Pa] represents the pressure, $\mathbf{I}$ is the unity matrix. The dynamic viscosity of the blood η [Pa·s] is dependent on the viscosity of plasma $\eta_{pl} = 1.35\times10^{-3}$ Pa·s and the hematocrit H [10]

$$\eta=\eta_{pl}\left(1+2.5H+7.37\times10^{-2}H\right). \tag{7}$$

The interaction between blood flow and the aortic structure is neglected due to the low deformations of large arteries [20, 21]; the arterial wall is then considered rigid. Aortic flow is limited at the aortic arch by an *inlet boundary* and similarly, at the abdominal level (lower limit of the computational domain) by an *outlet boundary*. An uniform, periodic velocity profile derived from the Womersley theory [22, 23] is set for the inlet, while a uniform, periodic pressure profile is assumed at the aorta outlet; the two profiles are shown in Fig. 4. The inlet velocity time-variation reproduces the shear rate profile (Fig. 3), according to (6). The flow problem solution gives the dynamic electrical conductivity for the electric field problem.

The electric field problem is solved next; the solution of an equivalent electro-kinetic model provides the data for the bioimpedance and its derivate waveforms computation. For low frequency (up to several hundred kilohertz) the tissues of the body are relatively good electric conductors, and their electric impedance can thus be considered dominantly resistive. Blood has a particularly high electrical conductivity

among other human tissues, and its dependency on the flow characteristics marks the general dynamics of the impedance determined in ECM. The electric field problem is thus solved for the electric potential V, in stationary working conditions (electro-kinetic regime, DC currents) and in magnetic vector potential **A**, in quasi-stationary working conditions (the actual procedure). The option for the equivalent DC problem is based on the difference between characteristic time scales of the two processes: the time scale for blood flow (slow process) is of the order $O(s^{-1})$ while the time scale for the electromagnetic field (fast process) is of the order $O(s^{-5})$. The two models are equivalent in the rms (root mean square) sense. Moreover, the advantage of using a companion DC model is that the pending algebra is related to real scalar quantities while for the harmonic model it is related to complex vector quantities.

1) *The Electro-kinetic Model* is described by Laplace equation for the electric potential V

$$\Delta V = 0. \tag{8}$$

The skin surface, representing the outer surface of the computational domain is considered electrically insulated and the condition $\mathbf{n}\cdot\mathbf{J} = 0$ is set, where $\mathbf{J}$ [A/m^2] is the electric current density, and $\mathbf{n}$ is the outward normal. All four electrodes are modeled as electric ports, as follows: *floating potential* conditions for the inner pair, and *inward current* and *ground* for the outer pair. All interior interfaces are implicitly set for electric field *continuity* conditions. The electro-kinetic model was applied by the authors in a previous study, reported as an intermediate step of the research project [18]. One more realistic model is formulated further for the electrical problem considered in the current analysis.

2) *The Quasi-Stationary Model* used in our study operates at f = 500 kHz; the penetration depth, approximated by $\delta = 1/\sqrt{\pi f \mu \sigma}$ indicates for human tissues values larger than the size of any anatomical domain (electrical conductivity $\sigma \sim 0.1\ldots0.001$ S/m and magnetic permeability of free space $\mu = \mu_0$; the coupling between the electric and magnetic fields in these circumstances may thus be neglected. The quasi-stationary problem is best solved using the complex representation formalism (complex quantities are marked with underlined symbols). Table 1 shows the electrical properties of the anatomical regions (tissues) and the corresponding penetration depths at 500 kHz; the properties (electrical conductivity σ, and dielectric constant ε_r) are compiled from the well-known database [24] and the penetration depth δ is computed as above.

Table 1

Electrical properties and penetration depth for anatomical regions (compiled from [24])

Region	σ [S/m]	ε_r	δ [m] at 500 kHz
Brain (averaged)	0.110	1050	2.147
Thorax (averaged)	0.044	3000	3.395
Liver	0.148	2770	1.851
Lungs	0.123	1025	2.030
Heart	0.281	3265	1.343
Blood	0.748	4189	0.823
Bone (averaged)	0.006	200	9.193

Because penetration depth is obviously larger than local length scale, the electric field is irrotational, which leads to $\underline{\mathbf{E}} = -\nabla \underline{V}$, where $\underline{V}$ is the complex representation of the electric potential. Based on the electric charge conservation law, $\nabla \cdot \underline{\mathbf{J}} = -\mathrm{j}\omega \underline{\rho}_v$, and the electric flux law, $\nabla \cdot \underline{\mathbf{D}} = \underline{\rho}_v$, the time-harmonic electric field produced by the sinusoidal current set through the current electrodes may be described then by the quasi-stationary diffusion model formulated by Ibanez et al. [25]

$$-\nabla\left[\left(\sigma + \mathrm{j}\omega\varepsilon_0\varepsilon_r\right)\nabla \underline{V} - \underline{\mathbf{J}}^e\right] = 0. \tag{11}$$

Here $\mathbf{D}$ [C/m^2] is the electric flux density, ρ_V [C/m^3] is the electric charge density, $\mathbf{J}^e$ [A/m^2] is the external electric current density, $\omega = 2\pi f$ [s^{-1}] is the angular frequency, ε_0 is the permittivity of the free space, and the complex number $\mathrm{j} = \sqrt{-1}$.

Same boundary conditions as for the electro-kinetic model are used: the surface of the thorax is assumed *electrically insulated* ($\mathbf{n}\cdot\mathbf{J} = 0$). The inner (current) electrodes have *floating potential* conditions, while the outer (voltage) electrode pair provides the *inward current* and *ground*, respectively. *Continuity* conditions are used for the interfaces between the anatomical regions.

4. RESULTS

The coupled problems were solved numerically by the finite element method (FEM) [11]. The hemodynamic problem was solved first and then the electric field problem. Several cardiac cycles were simulated before the periodic operation conditions (pulsatile flow) were reached. The results for the last hemodynamic cycle were used for the evaluation of the blood dynamic conductivity and the electric field analysis. The flow problem was FEM solved using quadratic Lagrange P1P2 elements, the electro-kinetic problem with Lagrange linear elements, and the quasi-steady electric field problem with first order vector elements.

Figure 5 shows the flow in the aorta (velocity arrows – a), and the electric current density in the thorax (flux tubes – b). Apparently the aorta is the highest electric current density path; any change in the blood conductivity due to the aortic flow should outline the flow dynamics. This process is echoed by the TEB.

Figure 6a displays, for reference, ECM experimental data shown by Vedru [26], using the usual inverse depiction of the TEB [27], while Fig. 6b shows the derived bioimpedance obtained using the numerical complex model presented here (flow associated with the electro-kinetic problem). Figure 6c compares two superposed waveforms for the time-derivative of the derived bioimpedance: one is the output of the electro-kinetic model and the other is computed with the quasi-stationary, harmonic model; the electrical conductivity presents the same dynamics, out of the flow problem.

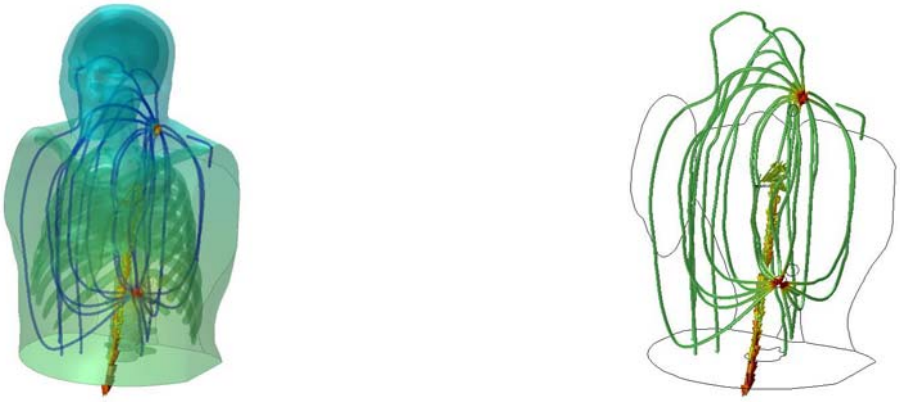

a) the electric potential (surface colored map) and the electric current flow (streamlines through the thorax).

b) the electric current density (streamlines) and the blood flow (arrows through the aorta).

Fig. 5 – Electric and flow analysis by ECM simulation with the coupled hemodynamic and electro-kinetic model.

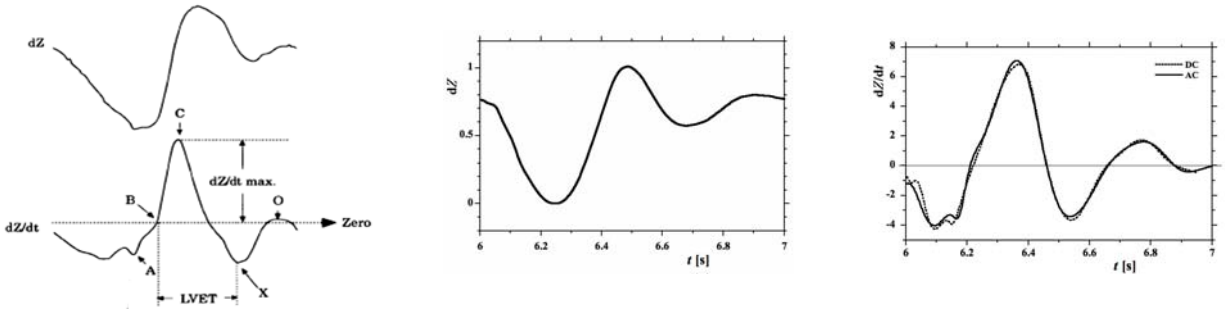

a) derived bioimpedance and its derivative (experimental data from [26]).

b) derived bioimpedance (numerical simulation with the DC model) – normalized w.r.t. its peak value.

c) time derivative of the derived bioimpedance (numerical simulation with both the DC and AC models).

Fig. 6 – TEB output resulted from measurements and simulations.

The waveforms obtained by numerical simulation of the TEB procedure look very similar to those acquired with the experimental setup [23, 26, 27]; the morphology of TEB and of its time derivative abide the expected trends, and confirm that the dynamics evidenced by ECM echoes the aorta hemodynamic. Several hemodynamic events identified and discussed in [23] are evidenced through the simulation too:

B – the beginning of ejection of blood by the left ventricle,
C – the major upward systole deflection,
X – the closure of the aortic valve,
O – the diastolic upward deflection,
LVET – the left ventricular ejection time,
dZ/dt_{max} – the maximum impedance change during systole.

Moreover, finer details, such as the A-wave emergence are also pinpointed, confirming the cardiac flow specificity stems, like the inlet flow profile used as boundary condition. The exact contributions of the right and left atria to the A-wave are under investigation. The A-wave seems to be linked to the contraction of the atria, but several sources suggest that it is produced by the back flow of blood from the atria into the central veins. It was found that the left atrium ejection might be the main cause of this wave, and the respective ejection fraction is significantly correlated to the amplitude of the A-wave.

Comparing the waveform of the time derivative of the derived impedance computed by the electro-kinetic model against the same type of waveform computed by the quasi-stationary model, one could observe their almost perfect resemblance (Fig. 6c); it is expected for the two models to give similar cardiovascular indices, which suggest that in what concerns numerical simulation, the harmonic regime may be replaced by the simpler electro-kinetic model without loss of accuracy. The explanation of this feature is the irrotational character of the electric field (skin depth larger than the length scales of the anatomical regions) and the significant discrepancy in the time scales of the blood flow dynamics and the high frequency of the ECM procedure.

6. CONCLUSIONS

This study highlights several aspects related to unobtrusive bioimpedance assessment in cardiology. Numerical analysis is performed for detecting and quantifying physiologic indices derived from electrocardiometry (ECM), specific to blood circulation correlated with the electrophysiology of the cardiac cycle. In numerical simulation related to medical problems, one major concern is usually the accuracy of the computational domain; a 3D realistic representation of the upper half of the body was reconstructed out of MRI images. The key point of connection between the electric field and the fluid flow numerical problems is the blood conductivity, presented through an equivalent quantity, obtained through averaging techniques out of analytical expressions. Several electrophysiology effects may not be assessed in the numerical model; for example, the nonlinear change in blood electrical conductivity for accelerating and decelerating flow is not considered, but the sensitivity of the solution to blood flow dynamics is clearly evidenced.

Thoracic bioimpedance and its derivative computed from ECM numerical simulation results compares satisfactorily well with available experimental data, and relevant flow parameters are clearly evidenced. Several cardiac hemodynamic indices useful in medical diagnosis become thus addressable: the start of ejection of blood by the left ventricle, the major upward deflection occurring during systole, the closure of the aortic valve, the diastolic upward deflection, the left ventricular ejection time and dZ/dt_{max}.

The electric field was modeled both under DC and AC operation conditions. Both provide practically the same ECM quantities, which suggests that AC regime may be replaced by the simpler DC model without loss of accuracy, in what concerns numerical simulation. The explanation of this feature is the irrotational character of the electric field and the significant discrepancy in the time scales of the blood flow and electric field dynamics.

This study was concerned with the direct problem of ECM bioimpedance with the aim to provide a mathematical and numerical model able to render the outlining physical processes that intervene in the ECM and to assess the sensitivity of TEB to the hemodynamic flow parameters. The results open the path to the inverse EMC-TEB problem, with the objective of showing the flow dynamics out of EMC bioimpedance data, which could be obtained from measurements.

ACKNOWLEDGMENTS

The authors acknowledge the logistic support offered by the Laboratory of Electrical Engineering in Medicine and BIOINGTEH Platform at the “Politehnica” University of Bucharest.

REFERENCES

1. Bernstein D.P., (2010) *Impedance cardiography: Pulsatile blood flow and the biophysical and electrodynamic basis for the stroke volume equations*, J. Electr. Bioimp., **1**, *1*, pp. 2–17, 2010.
2. Sathyaprabha T.N., Pradhan C., Rashmi G., Thennarasu K., Raju T.R., *Noninvasive Cardiac Output Measurement by Transthoracic Electrical Bioimpedence: Influence of Age and Gender*, J. Clin. Monit. Comput., **22**, *6*, pp. 401–408, 2008, doi: 10.1007/s10877-008-9148-6.
3. Funk D.J., Moretti E.W., Gan T.J., *Minimally invasive cardiac output monitoring in the perioperative setting. Anesth Analg*, **108**, *3*, pp. 887–897, 2009, doi: 10.1213/ane.0b013e31818ffd99.
4. Truijen J., van Lieshout J.J., Wesselink W.A., Westerhof B.E., *Noninvasive continuous hemodynamic monitoring*, J. Clin. Monit. Comput., **26**, *4*, pp. 267–278, 2012, doi: 10.1007/s10877-012-9375-8.
5. Ipate M.C., Dobre A.A., Morega A.M., *The Stroke Volume and the Cardiac Output by the Impedance Cardiography*, UPB Scientific Bulletin (Series C) **74**, *3*, pp. 219–232, 2012.
6. Osypka M., *An Introduction to Electrical Cardiometry*, Berlin, Germany, 2009, pp. 1–10. Electrical Cardiometry™ http://www.cardiotronic.net, accessed 30 January 2015.
7. Bernstein D.P., Osypka M.J., *Apparatus and method for determining an approximation of stroke volume and cardiac output of the heart*, US Patent No. 6.511.438, 2003, http://www.google.com/patents/US6511438, accessed 30 January 2015.
8. Mellert F., Winkler K., Schneider C., Dudykevych T., Welz A., Osypka M., Gersing E., Preusse C.J., *Detection of (Reversible) Myocardial Ischemic Injury by means of Electrical Bioimpedance*, IEEE Trans. Biomed. Eng., **58**, *6*, pp. 1511–1518, 2011, doi: 10.1109/TBME.2010.2054090.
9. Henry I.C., Bernstein D.P., Banet M.J., *Stroke Volume obtained from the Brachial Artery using Transbrachial Electrical Bioimpedance Velocimetry*, Proc 34th Int. Conf. IEEE-EMBS San Diego, California USA, 2012, pp. 142–145.
10. Hoetink A.E., Faes T.J.C., Visser K.R., Heethaar R.M., *On the Flow Dependency of the Electrical Conductivity of Blood*, IEEE Trans. Biomed. Eng., **51**, *7*, pp. 1251–1261, 2004, doi: 10.1109/TBME.2004.827263.
11. *** Comsol Multiphysics, AB, v. 3.5a, 4.2a, 2010–2012.
12. National Institutes of Health, *Visible Human Project*, U.S. National Library of Medicine, http://www.nlm.nih.gov/research/visible/visible_human.html, accessed 30 January 2015.
13. *** ScanIP, +FE and +CAD Reference Guide, Simpleware Ltd., UK, 2010.
14. *** Simpleware 4.2, Simpleware Ltd., UK, 2010.
15. Morega A.M., Dobre A.A., Morega M., *Blood Flow Indices Assessment by Electrocardiometry*, in: Ion S., Popa C. (ed.), *Topics of Mathematical Modeling of Life Sciences Problems*, MatrixRom, Bucharest, 2013, pp. 43–66.
16. Visser K.R., *Electric conductivity of stationary and flowing human blood at low frequencies*, Med. Biol. Eng. Compu., **30**, pp. 636–640, 1992, doi: 10.1109/IEMBS.1989.96329.
17. Gaw R.L., Cornish B.H., Thomas B.J., *The electrical impedance of pulsatile blood flowing through rigid tubes: A theoretical investigation*, IEEE Trans. Biomed. Eng., **55**, *2*, pp. 721–727, 2008, doi: 10.1109/TBME.2007.903531.
18. Morega A.M., Dobre A.A., Morega M., *Numerical Simulation in Electrical Cardiometry*, Proc 13th Int. Conf. on Optimization of Electrical and Electronic Equipment (OPTIM), Brasov, Romania, 2012, pp. 1407–1412.
19. Bejan A., *Heat Transfer*, J. Wiley & Sons Inc., New York, 1993, pp. 295–298.
20. Dobre A.A., Morega A.M., Morega M., *The Investigation of Flow – Structural Interaction in an Arterial Branching by Numerical Simulation*, IFMBE Proc. 10th IEEE Int. Conf. Information Technology and Applications in Biomedicine (ITAB), Corfu, Greece, 2010.
21. Morega A.M., Dobre A.A., Morega M., *Numerical Simulation of Magnetic Drug Targeting with Flow-Structural Interaction in an Arterial Branching Region of Interest*, Proc. Comsol. Users Conference Paris, France, pp. 17–19, 2010.
22. Dobre A.A., Morega A.M., Morega M., Ipate C.M., *Numerical Simulation in Electrocardiography*, Rev. Roum. Sci. Techn. – Électrotechn. et Énerg., **56**, *2*, pp. 209–218, 2011.
23. Taylor C.A., Hughes T.J.R., Zarins C.K., *Finite Element Modeling of Three-Dimensional Pulsatile Flow in the Abdominal Aorta: Relevance to Atherosclerosis*, Ann. Biomed. Eng., **26**, pp. 975–987, 1998.
24. Andreuccetti D., Fossi R., Petrucci C. (1997) *An Internet resource for the calculation of the dielectric properties of body tissues in the frequency range 10 Hz – 100 GHz*, IFAC-CNR, Florence (Italy), Based on data published by C. Gabriel *et al*. in 1996. http://niremf.ifac.cnr.it/tissprop, accessed 30 January 2015.
25. Ibanez L., Schroeder W., Ng L., Cates J., *The ITK Software Guide*, Second Edition, 2005.
26. Vedru J., *Electrical impedance methods for the measurement of stroke volume in man: state of art*, Acta & Comm UniTartuensis (Jartu, Estonia), **974**, pp. 110–129, http://kodu.ut.ee/~vedru/PUB/EImet_94.pdf, 1994, accessed 30 January 2015.
27. Woltjer H.H., Bogaard H.J., de Vries P.M.J.M., *The technique of impedance cardiography*, Eur. Heart. J., **18**, pp. 1396–1403, 1997.

Received June 4, 2015